CDF/PUB/TOP/PUBLIC/9234

Search for Heavy Top $t' \to Wq$ In Lepton Plus Jets Events

The CDF Collaboration
URL http://www-cdf.fnal.gov
(Dated: March 12, 2008)

We search for the heavy top (t') quark pair production decaying to Wq final states in 2.3 fb^{-1} of the CDF Run 2 data sample of lepton+jets. We reconstruct the mass of the t' quark and perform a likelihood of the observed (H_T, M_{reco}) distribution to discriminate the new physics signal from Standard Model backgrounds. We exclude a fourth-generation t' quark with a mass below 284 GeV at 95%CL.

Preliminary Results for Winter 2008 Conferences

I. INTRODUCTION

The topic of interest of this study is to investigate whether the present data allow or preclude the production of hypothetical new quarks which decay to final states with a high-p_T lepton, large $\not\!\!E_T$, and multiple hadronic jets, having large total transverse energy E_T, and thus mimicking top quark pair event signatures in the lepton+jets decay channel.

We performed previous iterations of this analysis using Run II datasets with integrated luminosities of 194 pb^{-1} [1], 347 pb^{-1} [2] and 760pb^{-1} [3]. In each of the latter two, several improvements were consecutively made to the technique in order to increase the sensitivity to new physics as detailed in the respective notes. The 760pb^{-1} analysis has been submitted to PRL [4] .

This current analysis uses 2.3 fb^{-1} of integrated luminosity, which corresponds to data taken up to August 2007.

We refer to the hypothetical new quark as t' for brevity, although such a signature could be a standard fourth-generation up-type heavy quark in which the splitting between the t' mass and the b' mass is less than the mass of the W boson (so that the decay is predominantly to Wq), as well as any up-type quark.

A fourth chiral generation of massive fermions with the same quantum numbers as ordinary ones is advocated in a number of models. It is favored by flavor democracy [5], for example, and arises by unifying spins and charges in the GUT SO(1,13) framework [6].

Precise measurements from LEP exclude light fourth neutrino ν_4 with mass $m(\nu_4) < m_Z/2$, where m_Z is the mass of the Z boson. On the other hand a fourth generation neutrino cannot be too heavy due to sizeable radiative corrections [7], although $m(\nu_4) \approx 100$ GeV/c^2 is still consistent with electroweak data [8]. If $m(\nu_4) \sim m_Z/2$ the radiative corrections become small [9], such a neutrino may explain some astrophysical puzzles [10], and then one extra chiral family of fermions with quark masses as high as 400 GeV/c^2 is viable [8, 17]. Additional fermion families can also be accommodated in two-Higgs-doublet scenarios and $N = 2$ SUSY models [16].

In all of the above scenarios the present bounds on the Higgs are relaxed; the Higgs mass could be as large as 500 GeV/c^2, with enhanced production at the Tevatron and LHC. In addition a small mass splitting between new heavy quarks t' and b' is preferred, such that $m(b') + m(W) > m(t')$, and that t' decays predominantly to Wq (a W boson and a down-type quark $q = d, s, b$) [11].

Other models with heavy exotic vector-like quarks decaying to Wq with vector couplings to the W boson are possible. Contributions to radiative corrections from such quarks with mass M decouple as $1/M^2$ and preserve the agreement with precision data. For example, the beautiful mirrors model [18] introduces a new fermion doublet, a mirror copy of the standard quark doublets with a heavier version of the standard model top decaying to Wb. This model improves the fit to the electoweak observables by eliminating the observed discrepancy in the $b\bar{b}$ forward-backward asymmetry [7, 19].

A heavy top-like quark also appears in Little Higgs (LH) models [20], which evade the hierarchy problem by introducing a minimal set of gauge and fermion fields in the context of a large-extra-dimension framework. In particular, LH models in which T-parity is conserved suggest a massive top-like quark which can decay to Wq as do LH models requiring two scales ($f_{1,2}$); these have been shown to prefer a toop-like quark having a mass of approximately 500 GeV [12, 13].

For the purposes of this analysis we make the following assumptions. The new quark

- is pair-produced strongly,
- has mass greater than the top quark, and
- decays promptly to Wq final states.

Due to the variety of theoretical models predicting similar signatures as well as the number of free parameters within each model, an a priori method was established to estimate the significance of a potential excess without attributing the events to a particular new physics model, but with the purpose of investigating them in more detail in another dedicated analsysis. Or, if no excess is observed, we set a limit on the fourth-generation t' quark pair production cross section (times branching ratio of $t' \to Wq$). However, other proposed models could have different kinematic distributions and acceptances than a generic fourth generation quark.

II. DATA SAMPLE AND EVENT SELECTION

The CDF detector is described in detail in [21]. We use a data sample corresponding to 2.3 fb^{-1} of integrated luminosity.

The following event selection criteria are applied

- one and only one high-p_T ($p_T \geq 20$ GeV/c) isolated electron or muon,
- large missing transverse energy ($\not\!\!E_T \geq 20$ GeV), and
- at least four energetic jets ($E_T \geq 20$ GeV when corrected for detector effects including multiple interactions).

The following additional cuts are applied to reduce the QCD background in our sample

- Cut in the $\Delta\phi$ between the corrected missing energy and the lepton vs missing energy plane: $\Delta\phi \geq A_1 - (1/B_1)\not\!\!E_T$ where $A_1 = 4.408$; $B_1 = 6.11$;
- Cut in the $\Delta\phi$ between the corrected missing energy and the leading jet vs missing energy plane: $\Delta\phi \geq A_2 - (1/B_2)\not\!\!E_T$ where $A_2 = 1.888$; $B_2 = 21.6$;
- Leading jet $E_T \geq 60$ GeV

The $\Delta\phi$ cuts were optimized with respect to top pair production. The cut on the leading jet E_T removes an additional 60% of QCD background while only removing a few percent of the signal.

To remove mis-measured muons with very high p_T we also require that the $\Delta\phi$ between the muon and the missing tranverse energy be ≤ 3.05.

Using these event selection criteria we observe a total of 1,118 events of which 667 contain an electron and 551 contain a muon.

The dominant contributing backgrounds after these cuts are from electroweak processes as well as $t\bar{t}$ pair production. Electroweak processes are dominated by W + jets, which we model with ALPGEN+Pythia. $t\bar{t}$ is modeled with PYTHIA. We assume the mass of the top quark to be 175 GeV. Other backgrounds include Z+jets, WW+jets, WZ+jets and single top which have a smaller rate than W + jets. Moreover thse other backgrounds are found to have similar kinematic distributions to W+jets and so are modeled as one using the W+jets model. The QCD background is modeled using a sample of data where the lepton ID cuts have been reversed.

III. ANALYSIS METHOD

We utilize the fact that the t' decay chain in the regime of interest is identical to the one of the top quark, the t' mass is reconstructed in the sam way as is done in the top quark mass measurement analyses. We use the template method for top quark mass reconstruction [22] based on the best χ^2-fit to the kinematic properties of final top decay products.

The χ^2 is given by the following expression:

$$\chi^2 = \sum_{i=\ell,4jets} \frac{(p_T^{i,fit} - p_T^{i,meas})^2}{\sigma_i^2} + \sum_{j=x,y} \frac{(p_j^{UE,fit} - p_j^{UE,meas})^2}{\sigma_j^2}$$

$$+\frac{(m_{jj} - m_W)^2}{\Gamma_W^2} + \frac{(m_{\ell\nu} - m_W)^2}{\Gamma_W^2} + \frac{(m_{bjj} - m_t)^2}{\Gamma_t^2} + \frac{(m_{b\ell\nu} - m_t)^2}{\Gamma_t^2}, \quad (1)$$

where the invariant masses of the W decay products m_{jj} and $m_{\ell\nu}$ are constrained to the pole mass of the W boson m_W, and the masses of top and anti-top (t' and $\bar{t'}$) quarks are required to be same. The Jet and lepton energies as well as the unclustered energy (UE) are allowed to float within their resolution uncertainties. The transverse component of the neutrino momentum is determined as the negative sum of the lepton, jet and unclustered transverse energies:

$$\vec{p}_T^{\,\nu} = -(\vec{p}_T^{\,\ell} + \sum \vec{p}_T^{\,jet} + \vec{p}_T^{\,UE}). \quad (2)$$

For each event there are total $4!/2 = 12$ combinations of assigning 4 jets to partons. In addition, there are two solutions to account for the unknown z-component of the neutrino momentum. After minimization of the χ^2 expression, the combination with the lowest χ^2 is selected and the value of m_t is declared to be the reconstructed mass M_{reco} of top (or t' respectively).

We use the observed distributions of the M_{reco} and total transverse energy in the event

$$H_T = \sum_{jets} E_T + E_{T,\ell} + \not\!\!E_T, \quad (3)$$

to distinguish the t' signal from the backgrounds by fitting it to a combination of t' signal, top, electroweak background, and QCD background shapes.

We use a binned in H_T and M_{reco} likelihood fit to extract the t' signal and/or set an upper limit on its production rate. We chose to use bins of 25 GeV in both H_T and M_reco with H_T in 26 bins from 150 to 800 GeV and M_reco in 16 bins from 100 to 500 GeV. The likelihood is defined as the product of the Poisson probabilities for observing n_i events in 2D bin i of (H_T, M_{reco}):

$$\mathcal{L}(\sigma_{t'}|n_i) = \prod_i P(n_i|\mu_i) \quad . \tag{4}$$

The expected number of events in each bin, μ_i, is given by the sum over all sources, indexed by j, which we further subdivide into separate e+jets and μ+jets sub-sources:

$$\mu_i = \sum_j L_j \sigma_j \epsilon_{ij} \quad . \tag{5}$$

Here L_j is the integrated luminosity, σ_j is the cross section, and ϵ_{ij} is the efficiency per bin of (H_T, M_{reco}).

We calculate the likelihood as a function of the t' cross section, and use Bayes' Theorem to convert it into a posterior density in $\sigma_{t'}$. We can then use this posterior density to set an upper limit on (or if we get lucky, measure) the production rate of t'.

The production rate for W+jets is a free parameter in the fit. Other parameters, such as the $t\bar{t}$ production cross section, lepton ID,data/MC scale factors, integrated luminosity, are related to systematic errors and treated in the likelihood as nuisance parameters constrained within their expected (normal) distributions.

We adopt the profiling method [1] for dealing with these parameters, i.e. the likelihood is maximized with respect to the nuisance parameters. The other (marginalization) technique, where the likelihood is integrated over all possible values of the nuisance parameters, is more CPU-intensive, but a cross check was performed and it gave consistent results. Taking this into account the likelihood takes the following expression:

$$\mathcal{L}(\sigma_{t'}|n_i) = \prod_{i,k} P(n_i|\mu_i) \times G(\nu_k|\tilde{\nu}_k, \sigma_{\nu_k}) \quad , \tag{6}$$

where ν_k are the nuisance parameters, such as $\sigma_{t\bar{t}}$, L_j and etc. $\tilde{\nu}_k$ are their central nominal values and σ_{ν_k} are their uncertainties. G is a Gaussian function centered at $\tilde{\nu}_k$ of width σ_{ν_k}

IV. SYSTEMATIC ERRORS

Jet Energy Scale

The sensitivity to t' depends on knowing accurately the distribution of (H_T, M_{reco}) in data. One of the largest sources of uncertainty comes from a factor that has a large effect on the shape of the kinematic distribution, the jet energy scale. Jets in the data and Monte Carlo (MC) are corrected for various effects as described in [23], leaving some residual uncertainty.

This uncertainty results in possible shifts in the H_T and M_{reco} distributions for both new physics and standard model templates. We take this effect into account by generating templates with energies of all jets shifted upwards by one standard deviation (+1 templates) and downwards (-1 templates) respectively.

We then use a template morphing technique that was developed in 2005 for a previous version of this analysis. We interpolate and extrapolate the expectation value μ_i at each bin i as follows:

$$\mu_i = \mu_{0,i} + \nu_{JES} \cdot (\mu_{+1,i} - \mu_{-1,i})/2 \tag{7}$$

where $\mu_{0,i}$ is the nominal expectation value, $\mu_{-1,i}$ and $\mu_{+1,i}$ are the expectation values from (-1) and (+1) templates respectively, and ν_{JES} is the nuisance parameter representing the relative shift in jet energy scale:

$$\nu_{JES} = \frac{\Delta_{JES}}{\sigma_{JES}} \quad . \tag{8}$$

$m(t')$	Q^2 scale		IFSR	
	offset	slope	offset	slope
180	0.61	0.016	0.125	0.026
200	0.72	0.018	0.125	0.024
220	0.48	0.025	0.125	0.022
240	0.36	0.022	0.110	0.020
260	0.20	0.027	0.080	0.018
280	0.12	0.028	0.060	0.017
300	0.093	0.022	0.035	0.014
320	0.072	0.021	0.025	0.011
340	0.055	0.016	0.015	0.009
360	0.043	0.014	0.010	0.008
380	0.033	0.011	0.007	0.007
400	0.025	0.011	0.005	0.006
450	0.015	0.007	0.004	0.005
500	0.013	0.006	0.003	0.004

TABLE I: Columns 2+3: Shift (in picobarns) in apparent t' cross section due to actual W+jets Q^2 scale being different from the nominal scale assumed, $Q^2 = m_W^2 + \sum_{jets} p_T^2$. Columns 4+5: Shift (in picobarns) in apparent t' cross section due to a shift in the initial- and final-state radiation up or down.

It enters the likelihood (6) as a Gaussian constraint penalty term: $G(\nu_{JES}|0,1) = \frac{1}{\sqrt{2\pi}} e^{-\nu_{JES}^2/2}$.

W+jets Q^2 Scale

The effect of the choice of the appropriate Q^2 scale for W+jets production is evaluated by measuring the resulting change in the measured t' cross section given that t' exists. The Q^2 scale is varied to $2Q^2_{nominal}$ and $\frac{1}{2}Q^2_{nominal}$ the expected change in the measured cross section is then interpreted as the uncertainty on the t' cross section itself. We measure this shift as a function of the t' cross-section by drawing pseudoexperiments from shifted templates and fitting them to the nominal distribution. The resulting shift is fitted to a linear function of that t' cross-section and is incorporated into the likelihood as an additive parameter to the t' cross section, so that the t' contribution to the expectation value μ_i (5) in bin i becomes

$$\mu_{i,t'} = L_{t'}(\sigma_{t'} + \nu_{Q^2})\epsilon_{i,t'} \quad , \tag{9}$$

where ν_{Q^2} is constrained by a gaussian with a width, that is a half of the largest of the upwards or downwards shifts for each mass of the t'.

The observed offsets and slopes for the linear fits to the t' cross-section for the different t' masses are shown in Table I

ISR and FSR

We varied the amount of initial- and final-state radiation together, i.e. shifting both up or both down. We generated samples with more ISR and FSR as well as some with less ISR and FSR. We refer to these samples as IFSR more and IFSR less. We generated samples for t' with masses of 250, 300 and 350 GeV which brackets the region where we expect to be able to place our exclusion limit.

The resulting effect is treated in a similar way to the Q^2 systematic. Templates are made for each of these mass points. Pseudoexperiments are thrown with the shifted top and t' IFSR samples, where the shift is set to be the same for top and t'. We then fit the obtained cross-section shift using a linear function of the t' cross-section.

The resulting shifts are shown in Table I. We add the resulting shifts in quadrature with the Q^2 error in the likelihood.

QCD Background

The QCD background shape is modeled from a sample of data in which the electron cuts have been reversed. The QCD normalization is obtained by fitting the background (electroweak, top, and QCD) distrubtions to the data with the missing E_T cut removed and then computing how much remains after all cuts are applied. As most of the QCD is expected to be found at low missing E_T.

We investigated using leptons that fail the isolation requirements to model our QCD background. This gave an excellent description of the jet E_T spectra but a very poor description of the lepton p_T distributions, which were much steeper in this model than expected from the data.

On the other hand the sample requiring the opposite of the electron cuts seems to give a reasonable description of most of the data kinematic distributions but has only very limited statistics; this means that the QCD templates need to be scaled up.

Cutting very hard on the leading jet E_T removes most of the QCD background which makes our fit rather insensitive to the QCD modeling.

The relative normalization uncertainty is taken to be 50%, as was done in the kinematic cross section analysis and the original $190pb^{-1}$ analysis, due to our lack of confidence in our model and normalization method. With our QCD veto cuts it turns out to change the fit by a negligible amount whether we constrain QCD or let it float. The uncertainty is represented by a Gaussian-constrained parameter in the likelihood. The QCD background has a negligible effect on the t' limit.

Integrated Luminosity

The integrated luminosity uncertainty is taken to be 5.9%, and is represented by an additional gaussian-constrained parameter multiplying all contributions except for the QCD background, which is normalized from data.

Lepton ID

We have two components for lepton ID. First is the efficiencies for the individual electrons and muons. We multiply each lepton type by the associated efficiency and gaussian constrain it within the error on the efficiency.

Second is the uncertainty on the lepton ID efficiency data/MC scale factor, which is of 2%, and taken as correlated across lepton types since it is due to the presences of multiple jets in an event. We add it in quadrature with the luminosity error, which is also correlated across lepton types, and include it with a gaussian constraint into the likelihood.

PDF Uncertainty

The Parton Distribution Functions (PDFs) are not precisely known, and this uncertainty leads to a corresponding uncertainty in the predicted cross sections, as well as the acceptance.

This effect is evaluated on both the top and the t' MC samples. The method consists in re-weighting the existing MC samples by the relative PDF weights given the parton momentum fractions (x_1, x_2) and Q^2 of the generated interaction.

46 eigenvectors are considered. We look at the difference between pairs of the CTEQ6M PDFs and add up these in quadrature. We then consider the difference between the two MRST72 and CTEQ5L PDF sets. If this is smaller than the 20 PDF sets uncertainty, we drop it. If it is larger, we add it in quadrature. To investigate the effect of α_s we look at the difference between the MRST72 and MRST75 PDF sets and add this in quadrature to the above errors.

The final PDF uncertaintes are given for each t' mass point as well as for top in Table II. A common conservative systematic error is added in quadrature to all other multiplicative factors and it taken as 1.1% for all templates.

Theory Uncertainty

The theory uncertainty in the t' cross section is about 10% (see Table III), which is mainly due to uncertainty in PDFs ($\sim 7\%$). The other effect comes from uncertainty in the choice of the Q^2 scale [15].

We take the theory uncertainty in $t\bar{t}$ cross section fully correlated with the one of $t'\bar{t}'$, and introduce it into the likelihood as a single nuisance parameter: $\nu_{theory} = \nu_{theory}(m'_t)$.

top		
175	+0.0110	-0.0112
tprime		
180	+0.007	-0.008
200	+0.004	-0.005
220	+0.005	-0.005
240	+0.003	-0.003
260	+0.003	-0.003
280	+0.002	-0.003
300	+0.001	-0.003
320	+0.001	-0.002
340	+0.002	-0.002
360	+0.003	-0.002
380	+0.002	-0.002
400	+0.005	-0.002
450	+0.004	-0.005
500	+0.015	-0.013

TABLE II: PDF uncertainty on top and t' calculated by reweighting the events according to the probability (given the various PDFs) of finding an up and down quark with appropriate momentum fractions.

$m(t')$ (GeV)	σ_{min} (pb)	σ_{center} (pb)	σ_{max} (pb)
180.0	4.9938	5.7476	6.2396
200.0	2.7815	3.1898	3.4525
220.0	1.5926	1.8236	1.9710
240.0	0.9299	1.0647	1.1515
260.0	0.5499	0.6302	0.6828
280.0	0.3281	0.3769	0.4096
300.0	0.1968	0.2268	0.2475
320.0	0.1183	0.1370	0.1502
340.0	0.0711	0.0828	0.0914
360.0	0.0426	0.0500	0.0555
380.0	0.0255	0.0301	0.0337
400.0	0.0152	0.0181	0.0204

TABLE III: Theory values of t' cross section for given mass [14, 15].

V. RESULTS AND CONCLUSION

We tested the sensitivity of our method by drawing pseudoexperiments from standard model distributions, i.e. assuming no t' contribution. The ranges of the expected 95% CL upper limits with one and two standard deviation bandwidth are shown in Figure 1.

The purple curve is the theoretical prediction [14, 15], the values of which are given in Table III. The lower σ_{min} and upper σ_{max} limits are obtained using the CTEQ6M family of parton density functions with uncertainties, together with the study of the scale uncertainty [24].

From Figure 1 it follows that given no t' presence, this method is on average sensitive to setting an upper limit at 284 GeV t' mass.

The red curve in Figure 1 shows the final result expressed as a 95% CL upper limit on the t' production rate as a function of t' mass. Table IV shows the individual calculated limites along with expected limits from pseudo-experiments for reference.

Based on these results we exclude at 95% CL a t' quark with mass below 284 GeV, given that the true top mass is 175 GeV. Of course, our measurement of the top mass may have been affected by the presence of a higher mass t'

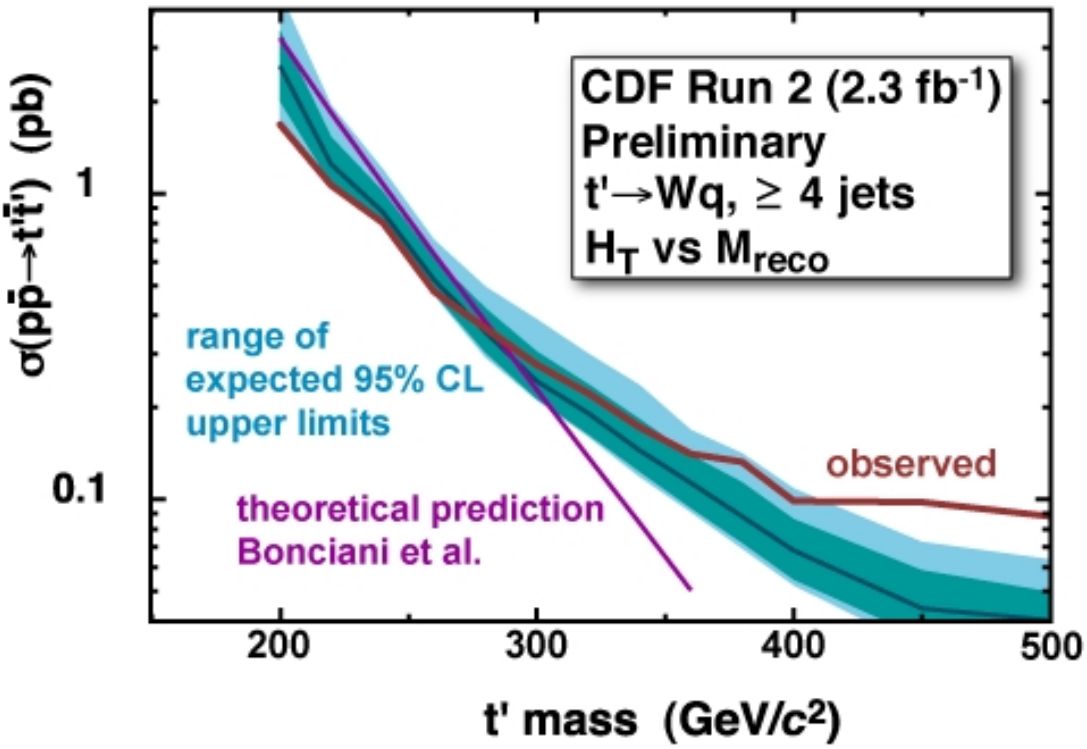

FIG. 1: Upper limit, at 95% CL, on the production rate for t' as a function of t' mass (red). The purple curve is a theoretical cross section. The dark blue band is the range of expected 95% CL upper limits within one standard deviation. The light blue band represents two standard deviations

	expected limit (pb)					**observed limit (pb)**
$m(t')$ **(GeV)**	-2σ	-1σ	**median**	$+1\sigma$	$+2\sigma$	
200	1.659	1.975	2.584	3.445	4.498	1.671
220	1.059	1.068	1.239	1.516	1.932	1.057
240	0.796	0.797	0.864	1.005	1.190	0.795
260	0.462	0.469	0.519	0.611	0.696	0.475
280	0.289	0.299	0.349	0.413	0.490	0.359
300	0.209	0.211	0.242	0.303	0.385	0.274
320	0.160	0.162	0.190	0.243	0.298	0.221
340	0.118	0.122	0.143	0.181	0.235	0.171
360	0.090	0.093	0.113	0.139	0.170	0.140
380	0.069	0.072	0.087	0.113	0.140	0.131
400	0.052	0.054	0.067	0.086	0.108	0.098
450	0.032	0.035	0.045	0.058	0.072	0.097
500	0.028	0.030	0.037	0.049	0.065	0.087

TABLE IV: Expected and obtained limits on t' production cross section for given mass.

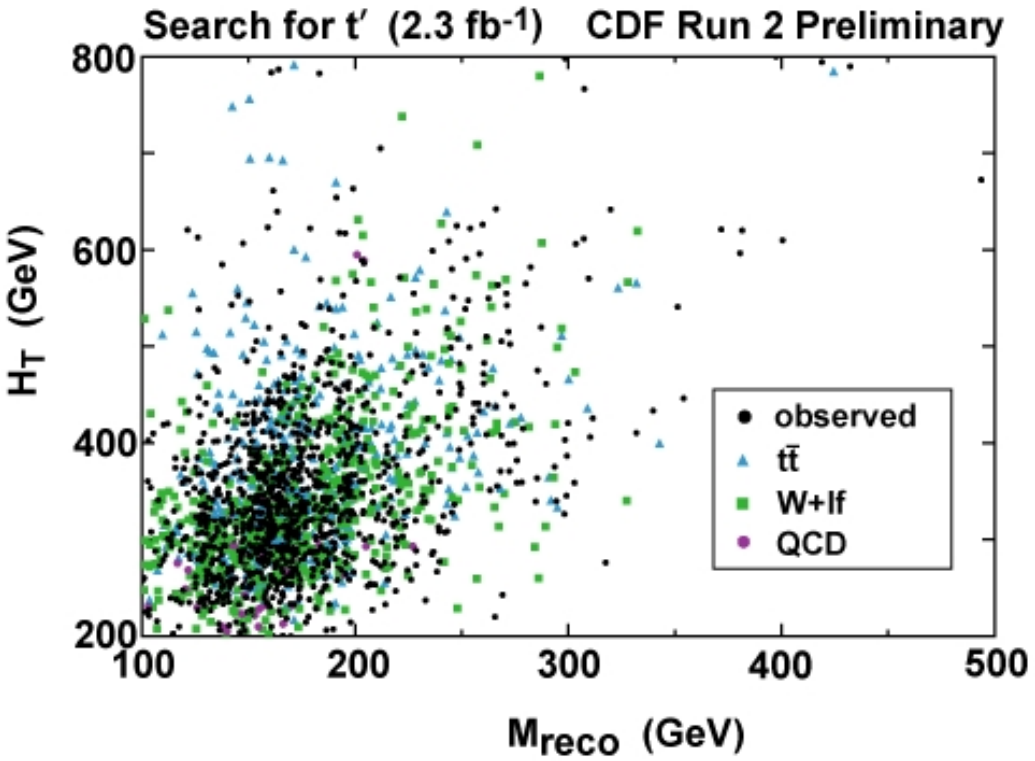

FIG. 2: 2D distribution of H_T vs M_{rec} distribution showing the data (black points) and the fitted number of background events: QCD (dark cyan triangles), W+jets (blue open circles) and $t\bar{t}$ (red triangles)

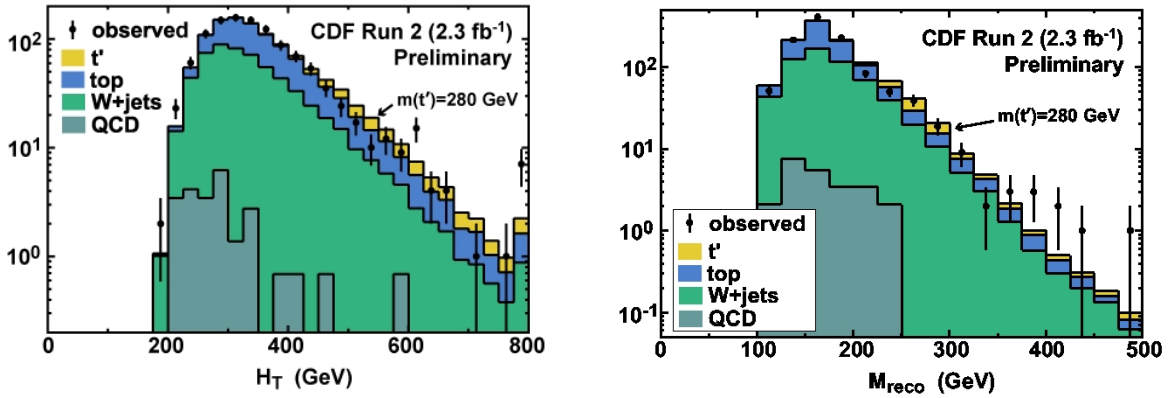

FIG. 3: H_T (left) & M_{reco} (right) distributions showing the results of the fit for m(t') = 280 GeV. The normalizations of the various sources and distortions of kinematic distributions due to systematic effects are those corresponding to the maximum likelihood when the cross section for t' is set to its 95% CL upper limit.

and thus we should treat these conclusions with care.

The 2D-distribution of (H_T, M_{reco}) is shown in Figure 2.

Distributions of H_T and M_{reco} showing the result of the fit for m(t')=280 GeV and no signal are shown in Figures 3 & 4

We checked the coverage of our 95% CL limit method for one t' mass, 300 GeV, as a function of the signal cross section. The method over-covers by a few percent for all cross-sections. This sort of behavior is not atypical of

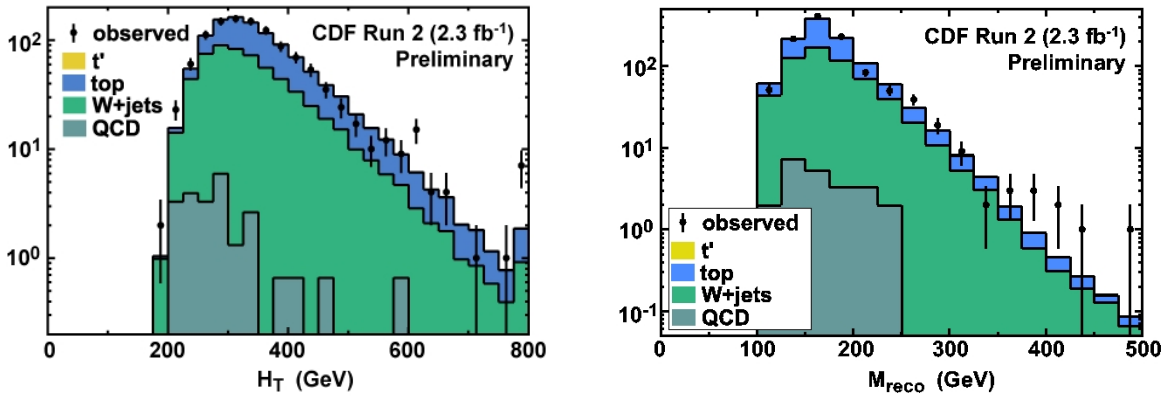

FIG. 4: H_T (left) & M_{reco} (right) distributions showing result of the fit for no signal. The normalizations of the various sources and distortions of kinematic distributions due to systematic effects are those corresponding to the maximum likelihood.

Bayesian methods.

To determine if the data show any evidence of an excess in the tails of H_T and M_{reco}, we decided *a priori* to count the number of events in groups of $n \times n$ of our standard 25 GeV bins in these quantities, and compare with the number predicted from a zero-signal fit to the full two dimensional spectrum. For each $n \times n$ bin one can then calculate the p-value for having observed that number or greater, given the prediction. If a significant effect is observed, one can calculate an overall p-value which is the probability that one would observe a p-value at least as significant as the most significant $n \times n$ bin or greater; this takes into account both the trials factor and the effect of systematic errors.

Table V shows the result of this counting experiment. The most significant $n \times n$ bin is for $n = 8$; the probability for observing 11 or more events given 4.694 expected is 0.0089. (This assumes systematic uncertainty on the background.) The overall p-value for observing an $n \times n$ bin with a significance this great or greater is 2.8%, which corresponds to a significance of $< 2\sigma$. Thus we conclude there is no statistically significant excess in the far tails of H_T and M_{reco}.

A. Event Displays of highest H_T and M_{rec} events

The 7 events with the highest values of H_T and M_{rec} are shown in Figures 6 to 12.

n	Min M_{rec} [GeV/c^2]	Min H_T [GeV]	observed	expected	p-value
1	475	775	0	0.0159	1.000
2	450	750	0	0.0626	1.000
3	425	725	1	0.1655	0.1525
4	400	700	2	0.2909	0.0349
5	375	675	3	0.5861	0.0218
6	350	650	4	1.231	0.0365
7	325	625	4	2.443	0.2302
8	300	600	11	4.694	0.0089
9	275	575	14	8.467	0.0501
10	250	550	23	15.52	0.0447
11	225	525	34	26.93	0.1055
12	200	500	49	44.77	0.2826
13	175	475	81	76.79	0.3304
14	150	450	128	133.2	0.6846
15	125	425	190	193.8	0.6159

TABLE V: Number of observed events in the highest $n \times n$ bins of H_T and M_{reco}, compared with the prediction from a zero-signal fit to the full spectrum. For each value of n, the table shows the p-value, the probability for observing at least what was actually observed or more, given the number expected. The minimum H_T and M_{rec} in each trial are also shown.

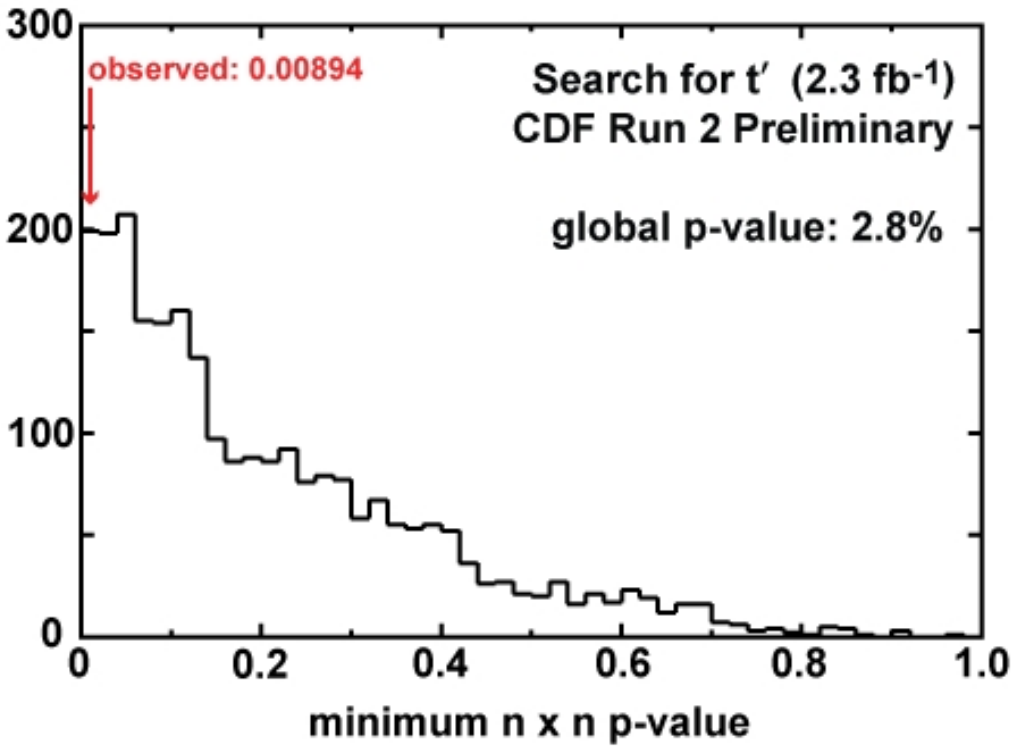

FIG. 5: Pseudoexperiment distriubtion of the smallest p-value of all of the nxn bins. The integral of this distribution from zero up to the observed minimum p-value 0.0089 gives the global p-value, 0.028.

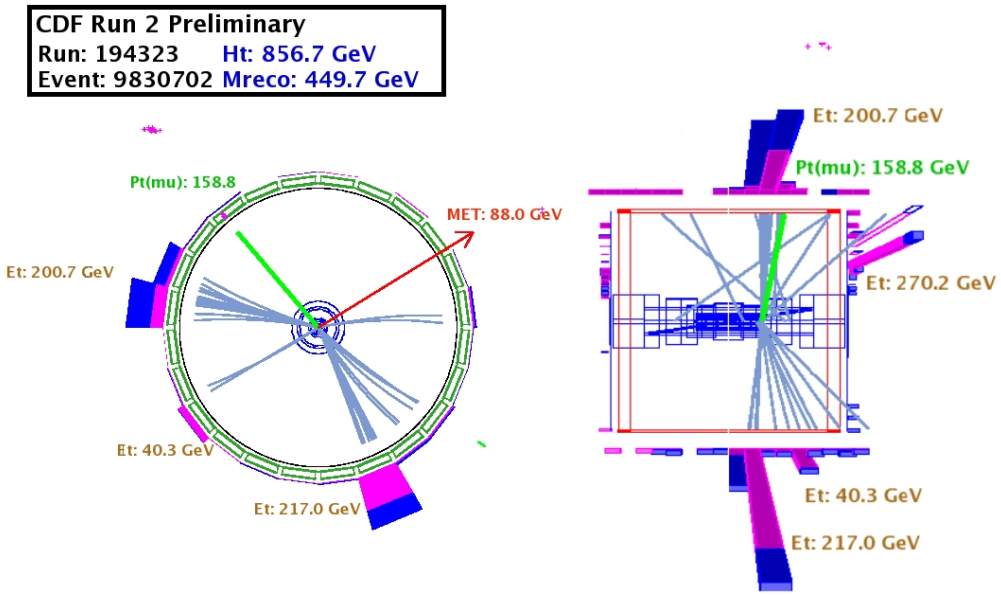

FIG. 6: Event display for Run Number 194323, Event Number 9830702

[1] J. Conway *et al.*, CDF Public note 7113.

[2] J. Conway *et al.*, CDF Public note 7912.

[3] J. Conway *et al.*, CDF Public Note 8495.

[4] CDF Collaborataion: T. Aaltonen *et al.* [arXiv:hep-ex/08013877].

[5] J. Silva-Marcos JHEP 0212 (2002) 036, [arXiv:hep-ph/0204217]; S. Sultansoy *et al.* , Acta Phys.Polon. **B37** (2006) 2839-2850, [arXiv:hep-ph/0502050]

[6] N. Borstnik *et al.*, Bled workshops in physics, Vol.7, No. 2, DMFA-Zaloznistvo, Ljubljana, Dec. 2006, [arXiv:hep-ph/0612250].

[7] J. Erler *et al.* [Particle Data Group Collaboration], Phys. Lett. **B592** (2004) 1.

[8] G. Kribs *et al.* ANL-HEP-PR-07-39 (2007).

[9] M. Maltoni *et al.*, Phys. Rev. Lett. **B476** (2000) 107, [arXiv:hep-ph/9911535].

[10] D. Fargion *et al.*, JETP Lett. 69 (1999) 434-440, [arXiv:astro-ph/9903086]; [arXiv:astro-ph/0411093].

[11] P.Frampton, P. Hung, and M. Sher, Phys. Rept. 330, 263 (200).

[12] H. C. Cheng and I. Low, J. High Energy Phys. **0408**, 61 (2004)

[13] D. E. Kaplan and M. Schmaltz, J. High Energy Phys. **0310**, 39 (2003); R. Barcelo, M. Masip, and M. Moreno-Torres, arXiv:hep-ph701040.

[14] R. Bonciani, S. Catani, M. L. Mangano and P. Nason, Nucl. Phys. B **529** (1998) 424 [arXiv:hep-ph/9801375].

[15] M. Cacciari, S. Frixione, M. L. Mangano, P. Nason and G. Ridolfi, JHEP **0404** (2004) 068 [arXiv:hep-ph/0303085].

[16] H.-J. He, N. Polonsky and S. Su, [arXiv:hep-ph/0102144]

[17] L. Okun *et al.*, [arXiv:hep-ph/0111028]

[18] C. Wagner *et al.*, [arXiv:hep-ph/0109097]

[19] LEP Electroweak Working Group, LEPEWWG/2001-01. M. Chanowitz, Phys. Rev. Lett. **87**, 231802 (2001), [arXiv:hep-

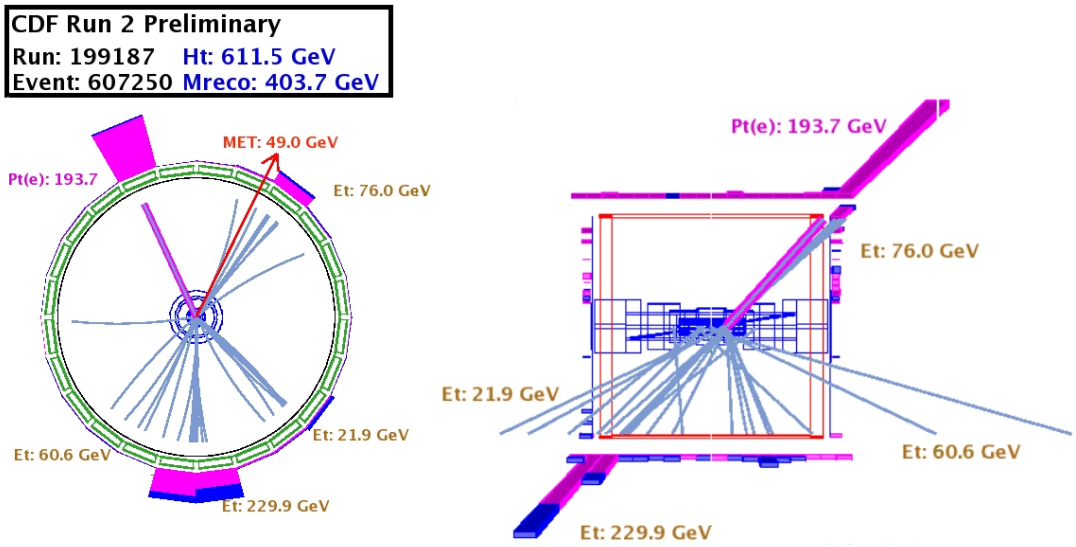

FIG. 7: Event display for Run Number 199187, Event Number 607250

ph/0104024].

[20] T. Han, *et al.*, Phys. Lett. B563:191 (2003).

[21] F. Abe, et al., Nucl. Instrum. Methods Phys. Res. A **271**, 387 (1988); D. Amidei, et al., Nucl. Instum. Methods Phys. Res. A **350**, 73 (1994); F. Abe, et al., Phys. Rev. D **52**, 4784 (1995); P. Azzi, et al., Nucl. Instrum. Methods Phys. Res. A **360**, 137 (1995); The CDFII Detector Technical Design Report, Fermilab-Pub-96/390-E

[22] A. Abulencia *et al.*, Phys. Rev. D **73**, 032003 (2006)[arXiv:hep-ex/0510048].

[23] A. Bhatti *et al.*, Submitted to Nucl. Instr. Meth. A [arXiv:hep-ex/0510047].

[24] Personal communication with Michelangelo Mangano.

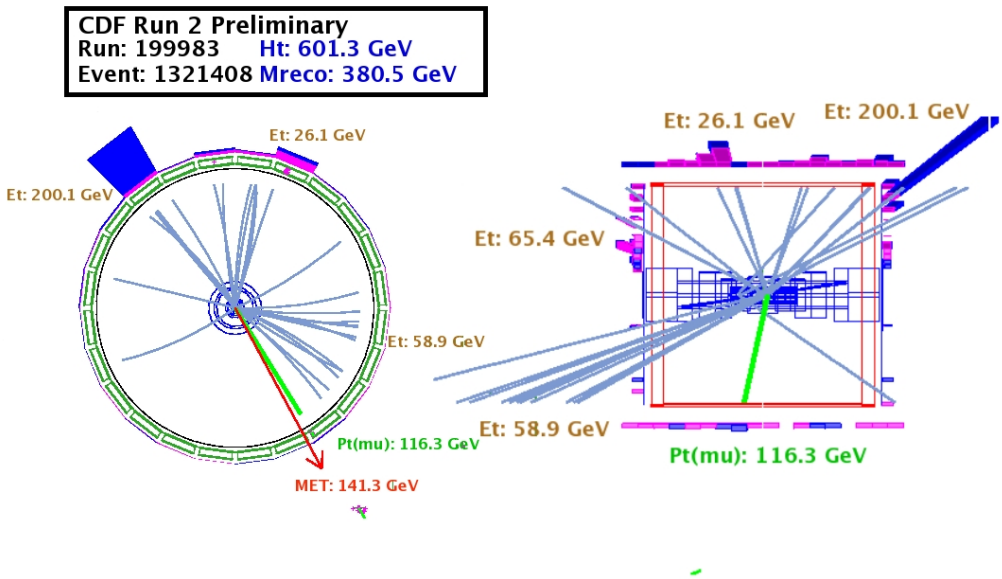

FIG. 8: Event display for Run Number 199983, Event Number 1321408

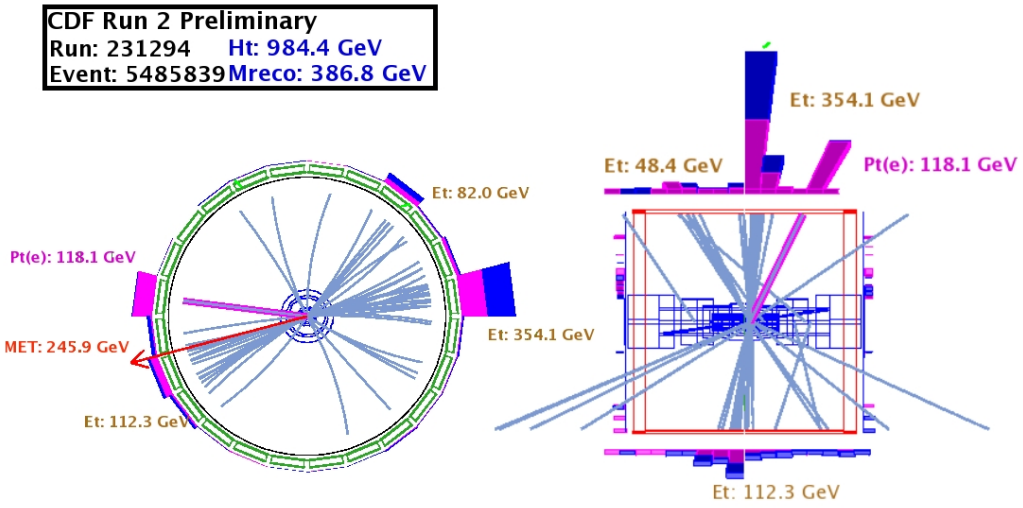

FIG. 9: Event display for Run Number 231294, Event Number 5485839

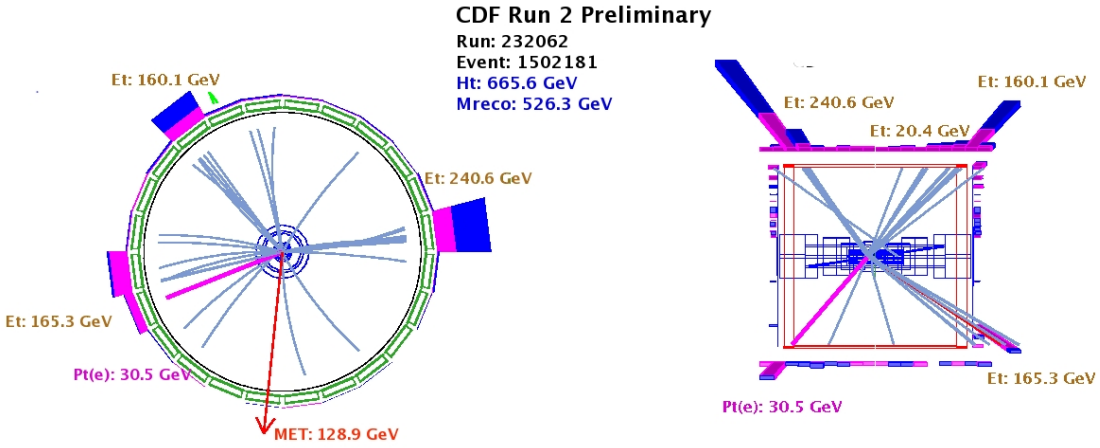

FIG. 10: Event display for Run Number 232062, Event Number 1502181.

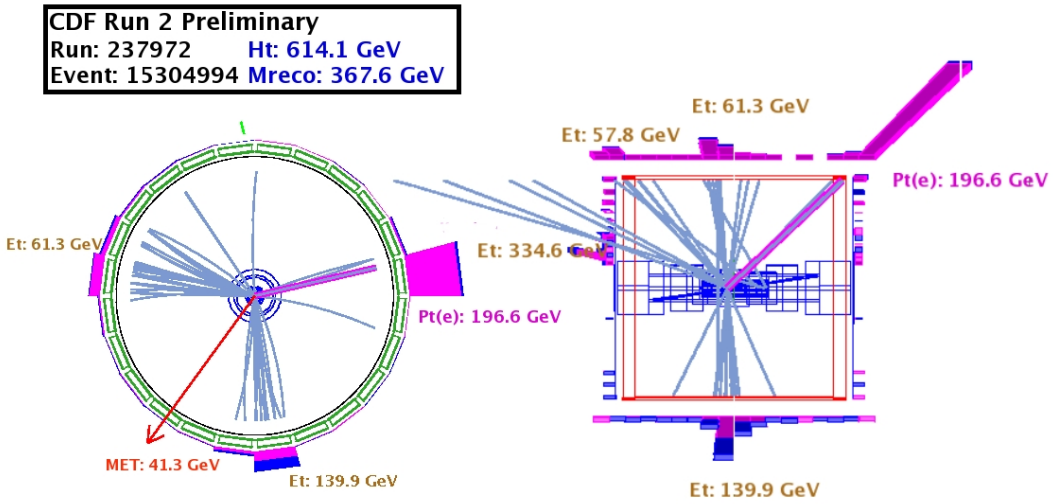

FIG. 11: Event display for Run Number 237972, Event Number 15304994.

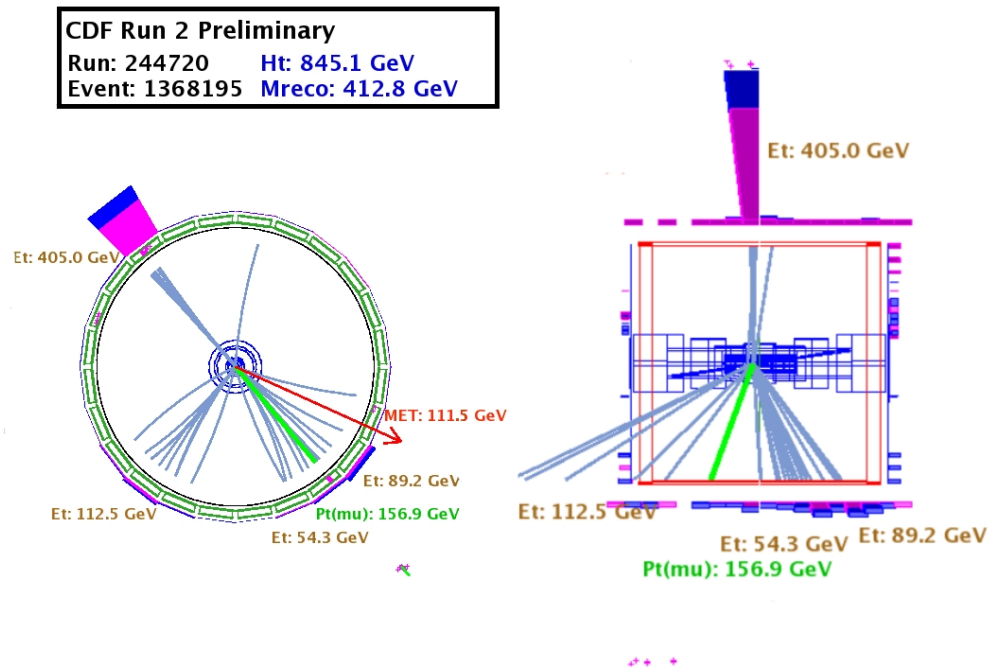

FIG. 12: Event display for Run Number 244720, Event Number 1368195.